



## Coexistence of one-dimensional and two-dimensional topology and genesis of Dirac cones in the chiral Aubry-André model

T. V. C. Antão <sup>1,2</sup>, D. A. Miranda <sup>3</sup>, and N. M. R. Peres <sup>3,4,5</sup>

<sup>1</sup>*Department of Applied Physics, Aalto University, 02150 Espoo, Finland*

<sup>2</sup>*Laboratorio de Instrumentação e Física Experimental de Partículas, University of Minho, 4710-057 Braga, Portugal*

<sup>3</sup>*Centro de Física das Universidade do Minho e do Porto (CFUMUP) e Departamento de Física, Universidade do Minho, P-4710-057 Braga, Portugal*

<sup>4</sup>*International Iberian Nanotechnology Laboratory (INL), Av Mestre José Veiga, 4715-330 Braga, Portugal*

<sup>5</sup>*POLIMA - Center for Polariton-driven Light-Matter Interactions, University of Southern Denmark, Campusvej 55, DK-5230 Odense M, Denmark*



(Received 8 January 2024; revised 16 May 2024; accepted 17 May 2024; published 31 May 2024)

We construct a one-dimensional (1D) topological SSH-like model with chiral symmetry and a superimposed hopping modulation, which we call the chiral Aubry-André model. We show that its topological properties can be described in terms of a pair  $(C, W)$  of a two-dimensional (2D) Chern number  $C$ , stemming from a superspace description of the model, and a 1D winding number  $W$ , originating in its chiral symmetric nature. Thus, we showcase the explicit coexistence of 1D and 2D topology in a model composed of a single 1D chain. We detail the superspace description by showcasing how our model can be mapped to a Harper-Hofstadter model, familiar from the description of the integer quantum Hall effect, and analyze the vanishing field limit analytically. An extension of the method used for vanishing fields is provided in order to handle any finite fields, corresponding to hopping modulations both commensurate and incommensurate with the lattice. In addition, this formalism allows us to obtain certain features of the 2D superspace model, such as its number of massless Dirac nodes, purely in terms of topological quantities, computed without the need to go into momentum space.

DOI: [10.1103/PhysRevB.109.195436](https://doi.org/10.1103/PhysRevB.109.195436)

### I. INTRODUCTION

Quasicrystals, once the subject of controversy, have now been firmly established as intriguing materials that defy the classification of traditional crystals. Indeed, their mathematical description was proposed a long time before their actual observation in 1982 and subsequent publication in 1984 [1]. Since then, many forms and realizations of quasicrystals have been reported [2]. One reason for interest is that they evade the classification of usual crystals based on symmetries of their underlying discrete translation groups, but nonetheless are “ordered” in a translational sense [3,4]. In the present day, it has long been realized that quasicrystals in  $d$ -dimensional space can be thought of as crystalline structures living in a higher  $d + d'$  dimensional superspace, which are projected down to a physical dimension, and this feature has been utilized to explore the properties of topological quasicrystals.

The method used for the projection can be picked from a variety of approaches, the most common of which may be the so-called “cut and project” method [5,6], which is at the heart of the most famous quasicrystalline structures, such as the Fibonacci quasicrystal, which can be realized as a projection from a 2D superspace lattice into a 1D chain [7], or the Penrose tiling, which is a two-dimensional slice of a five-dimensional hypercubic superspace lattice [8]. Different approaches include a “twisting” approach, based on coupling and twisting of monolayers of certain materials into twisted van der Waals heterostructures, such as

twisted-bilayer graphene [9], for which incommensurability has been studied and is argued to be an important feature [10,11].

In some approaches, one actually starts with a crystalline structure in the physical space, upon which some periodic potential incommensurate with the lattice is added, allowing the unfolding of the model into a higher superspace description. This “incommensurate potential” method is at the heart of the so-called Aubry-André (AA) models [12,13].

The fact that quasicrystalline structures, such as AA models, can host nontrivial single-particle as well as many-body topology is one of their most captivating aspects, from both technological and theoretical perspectives. On the theory side, it has been pointed out that the existence of phasonic excitations or degrees of freedom corresponding, for instance, to momenta along synthetic dimensions in superspace can be used to physically realize  $d + d'$ -dimensional topological invariants in  $d$ -dimensional systems [14–17].

The standard example of this feature is the presence of the two-dimensional (2D) Chern number in a one-dimensional (1D) AA model. Much like the “cut and project” approach, where deformations of the cutting window induce additional mechanical degrees of freedom, shifting an AA potential relative to the lattice also corresponds to a so-called phasonic degree of freedom, and a 2D superspace crystal can be built by interpreting this phason as a momentum coordinate. This occurs because a periodic potential of this kind can be thought of as unfolding the model into a series of replicas

and generating hoppings between them. The resulting lattice exists in one dimension higher, and the additional dimension is said to be “synthetic”. The periodicity of the potential is mapped to the magnitude of a “magnetic field” applied to the higher-dimensional lattice, which induces Peierls phases when hopping along the synthetic dimension. Thus, the superspace model of the AA model maps to a square lattice hosting integer quantum Hall effect (IQHE) physics [18,19], where transverse conductance is well known to be topologically characterized by the Chern number [20,21]. Beyond these simple models, the superspace picture and phasonic degrees of freedom have also been used to characterize the many-body topology of quasicrystals [22], where it is the topological terms, which can appear in a Lagrangian describing the elastic and phasonic deformations of the superspace lattice that determine the possible topological properties of the model.

The remarkable feature of quasicrystals we deal with here, is that any physical quasicrystal model retains some of the topological properties of the superspace model. This can be readily verified by analyzing the spectrum and eigenstates of the AA model, which can be seen to clearly exhibit finite energy states localized at the edges. Furthermore, these are a direct consequence of the topological properties of the presence of a Chern invariant. This crucial point has been studied experimentally in the context of photonic crystals using waveguide arrays within dielectric media [14].

Besides quasicrystals, chiral symmetric models have also been shown to host extremely rich topology, and a propensity for generalization into different topological models via a process of stacking. Chern numbers characteristic of 2D matter can, for instance, exist in certain quasi-1D models subject to magnetic fields, such as the Creutz-Su-Schrieffer-Heeger (CSSH) models [23], constructed by stacking two SSH chains in a square configuration, and connecting them with diagonal (second nearest neighbor) as well as vertical (nearest neighbor) bonds.

Additionally, stacking multiples of these SSH chains, repeating the Creutz-ladder pattern in the 2D plane or 3D space, one can construct Weyl-semimetals in 2D and 3D [24], and when certain types of interactions are turned on, these systems have even been shown to host topological superconducting properties [25]. In such previous studies, AA-type models are considered; however, in order to analyze the spectra and other properties of these systems, modulations have always been considered to be commensurate with the lattice.

It has furthermore been shown that incommensurate disorder can drive an SSH model from a trivial into an Anderson topological insulator phase [26].

We argue here that the idea of stacking topological models of low dimension into a higher-dimensional model is not dissimilar from the aforementioned superspace description of quasicrystals, and thus the presence of 2D Chern numbers in ladder systems or 1D models stacked along a second dimension, the rich landscape of SSH-type chiral symmetric models, as well as previous study suggesting the possibility of cross dimensionality of topological properties due to periodic drives [27] are suggestive of a question: Is it possible to construct a topological crystalline existing physically in the form of a single 1D chain, and via modulating using an AA approach, render it doubly topological? Or in other words, can the AA

modulation of a chiral symmetric model lead to the coexistence of 1D and 2D topology in a model in 1D physical space?

We show in this paper that topological invariants characteristic to different dimensionalities can coexist in a physically meaningful and experimentally testable fashion in a model we call the chiral Aubry-André model (cAA), extending previous study on this subject into the fully incommensurate setting. The cAA is perhaps one of the simplest conceivable candidates for such a coexistence of 1D and 2D topology, as it is built from the SSH model [28], which exhibits topological properties protected by chiral symmetry. In particular, the SSH model hosts a quantized topological invariant corresponding to the winding number  $W$ .

In order to build the cAA, to the SSH model, an off-diagonal Aubry-André (odAA) term is added. This results in a quasiperiodic modulation of the hopping amplitudes. Global shifts in this modulation correspond to phasonic degrees of freedom, providing the ground for the topological enrichment of the model. A schematic illustration of the cAA model is presented in Fig. 1.

Experimental realization of our model using platforms such as photonic crystals should not be out of reach, since the actual methodology as utilized, by Kraus *et al.* [14] (see Fig. 2), for instance, could easily be adapted to account for the different structure of hopping modulation necessary to implement the cAA system. Many alternative platforms exist, which may realize the cAA model, such as twisted bilayer graphene with adhered hydrogen or deuterium atoms. This has been proposed in the past as a way to generate and tune the modulation of a  $S = 1/2$  Aubry-André-Heisenberg chain [29].

In the simplest cases where the unperturbed model has no special symmetry, the odAA model has been shown to be topologically equivalent to the AA model by using a superspace prescription. Its topology is entirely characterized by the same Chern number  $C$ , in the same manner as the traditional AA model, and indeed, a topological equivalence to the Fibonacci quasicrystal has also been established [30].

In our cAA model, however, the presence of chiral symmetry in the original model actually breaks the topological equivalence between AA and odAA models, since an on-site disorder term would break this chiral symmetry, and therefore a change is observed in the Altland-Zirnbauer symmetry class of the 1D model.

As showcased in the typical example of the dispersion of the cAA model in Fig. 2(b), a series of puzzling characteristics appear, such as zero-energy edge modes, and finite-energy edge states connecting bulk bands.

The aim of this paper is mainly to provide a unified topological treatment of these features, relating them back to a pair of topological invariants  $(C, W)$ , allowing for an explanation of the aforementioned topological equivalence by noting that by breaking chiral symmetry  $W$  becomes an ill-defined quantity.

Furthermore, the relative simplicity of the cAA model results in the possibility of obtaining analytical expressions for the spectrum in the limit of vanishing field (large periodicity for the AA modulation). By constructing the superspace model as showcased in Fig. 2(b), and working within this limit, we show that an additional series of interesting features

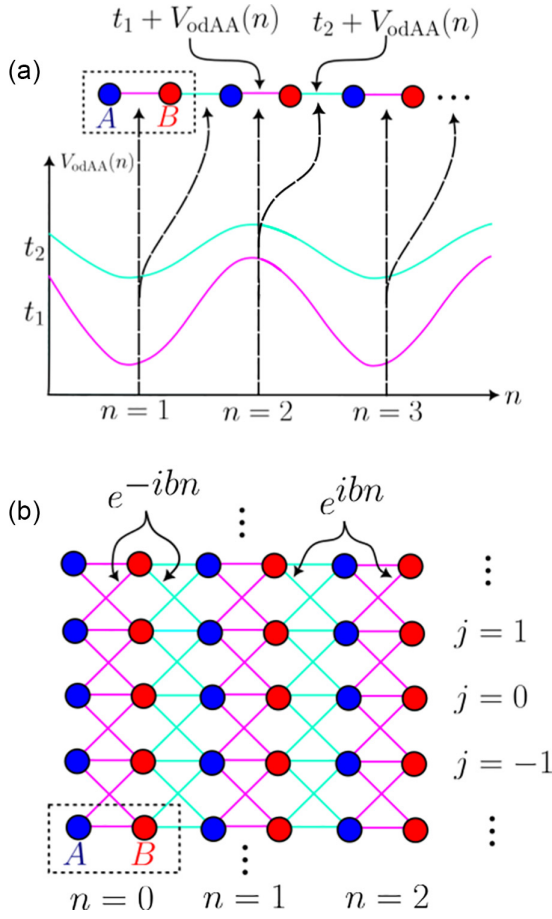


FIG. 1. (a) Schematic of the cAA model accompanied by an example plot of the co-sinusoidal hopping amplitude modulation of the underlying SSH model  $V_{\text{odAA}}(n)$  as a function of the lattice site. (b) Illustration of the corresponding model using a synthetic dimension, capturing all possible phasonic shifts of the Aubry-André potential. Blue and red circles in either panel correspond to the A and B sublattice sites respectively, horizontal lines connecting the sites indicate the physical hoppings, and diagonal lines connecting adjacent copies of the model are generated by the presence of the incommensurate hopping modulation. Hoppings connecting replicas of the 1D chain are accompanied by Peierls phases  $e^{\pm ibj}$ , where the inverse modulation periodicity  $b$  plays the role of an applied magnetic field.

appear, such as the genesis of a variable and tunable number of anisotropic massless Dirac cones. The Dirac cones can be fused together by changing the model’s relative hopping and modulation magnitudes, allowing for phase transitions between topological semimetal, topological insulator, and trivial insulator phases. The phenomenology and physics of Dirac cones is interesting in its own right, being responsible for the spur of research in many quantum materials, such as graphene. This carbon-based 2D material naturally hosts Dirac fermions [31]. Furthermore, in graphene, it is well known that the presence of two Dirac cones leads to a quantization of conduction at half-integer multiples of  $e^2/h$  (where  $e$  is the electron charge and  $h$  is Planck’s constant) when an external magnetic field is applied. This effect is often called the half-integer quantum Hall effect (HIQHE).

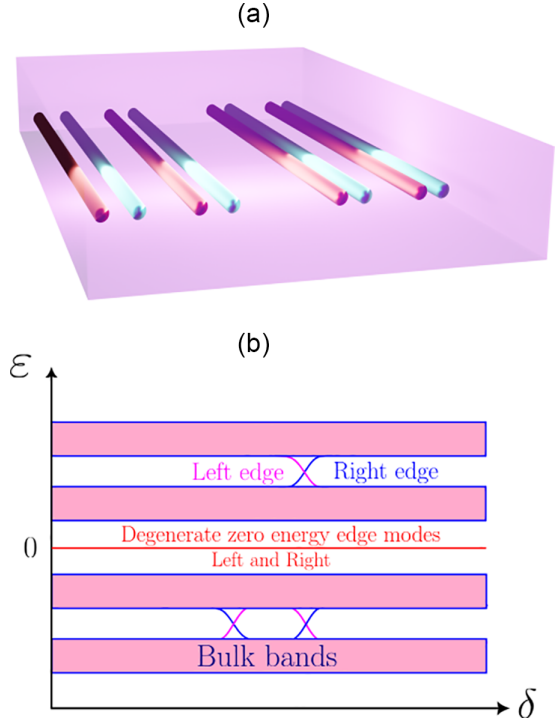


FIG. 2. (a) Artistic rendition of the realization of the cAA model in a photonic crystal platform. The physical spacing between adjacent waveguides is tuned to take into account both the SSH and odAA modulations. (b) Typical example plot for the spectrum of the superspace cAA model with an incommensurate potential. The presence of doubly degenerate zero-energy edge modes along with edge states at finite energies points to the main results of this paper: the coexistence of 1D and 2D topology in a purely 1D model.

On the other hand, in the absence of Dirac cones, a magnetic field induces a quantization of conductance at integer multiples of  $e^2/h$ , resulting in the integer quantum Hall effect (IQHE) instead.

In the cAA model, when considering hopping modulations of large yet finite wavelengths, the genesis of Dirac cones in the superspace cAA model, together with the ability to induce semimetal to insulator or nodal line semimetal phase transitions, results in the possibility of simulating both the HIQHE and IQHE.

Finally, changing properties such as phasonic degrees of freedom is found to be an extremely useful knob for the study and applications of topologically protected edge modes. In particular, we show that shifting the phason allows for turning these modes on or off, both at zero and finite energy in the 1D physical realization of the model, as well as change at which physical edge of the system they appear in.

The remainder of this paper is organized as follows: In Sec. II we give some details on our definition and construction of the chiral Aubry-André model, in Sec. III we analyze the topological 1D and properties of the energy spectrum from the point of view of the superspace model in the limit of vanishing field (long wavelength odAA modulations). We also discuss a way to calculate the number of massless Dirac cones by counting changes in the winding number as the momentum in the synthetic direction is traversed. In Sec. IV we extend our

discussion to the presence of finite fields, and using topological markers [32–36], explicitly showcase the coexistence of topological invariants in the incommensurate limit, extending our computations of the number of Dirac cones to the case when the periodicity of the odAA term explicitly breaks the translational symmetry of the model.

## II. THE CHIRAL AUBRY-ANDRÉ MODEL

The main aim of this paper is to showcase a toy model, which is topologically nontrivial in character from the outset, but which under the presence of an AA-type incommensurate modulation exhibits enriched topological properties, stemming from its superspace description. In this section, we motivate and build such a model. Let us consider what is arguably the simplest 1D topologically nontrivial model: the SSH model. This model is in the BDI class of the Altland-Zirnbauer classification of topological invariants [37,38], wherein a  $\mathbb{Z}$ -valued topological invariant is well defined, and often referred to as the winding number. The quantization of this winding number is assured by the presence of two distinct sites per unit cell, of type *A* and *B*, or equivalently by the existence of two sublattices, together with hopping terms, which connect only *A*-type sites to *B*-type sites and vice versa. This latter condition can, in fact, be thought of as the definition of chiral symmetry (which for this reason sometimes referred to as sublattice symmetry). For simplicity, we shall assume that the fundamental length scale, corresponding to the lattice spacing is  $a = 1$  in natural units, such that the SSH Hamiltonian reads

$$H_{\text{SSH}} = - \sum_n t_1 a_n^\dagger b_n + t_2 b_n^\dagger a_{n+1} + \text{H.c.}, \quad (1)$$

where  $a_n^\dagger$  ( $a_n$ ) create (annihilate) excitations in the *A* sublattice within the unit cell  $n$ , and equivalently for  $b_n^\dagger$  ( $b_n$ ) in the *B* sublattice.  $t_1$  represents the intracell hopping strength, and  $t_2$  the intercell hopping. The topological properties of the model crucially rely on the presence of chiral symmetry, and quantization of the winding number is robust to perturbations only if the added perturbations themselves respect this symmetry. If we wish to design a model with an additional topological invariant, we must therefore preserve chiral symmetry. To achieve this, an off-diagonal Aubry-André (odAA) hopping modulation is considered, given by the expression

$$H_{\text{odAA}}(\delta) = - \Delta_1 \sum_n \cos(2\pi bn - \delta) a_n^\dagger b_n + \text{H.c.} \\ - \Delta_2 \sum_n \cos(2\pi bn - \delta) b_n^\dagger a_{n+1} + \text{H.c.}, \quad (2)$$

where the parameters  $\Delta_1$  and  $\Delta_2$  denote the strengths of the modulation in intracell and intercell hoppings, respectively. The modulation occurs periodically with a period  $L = 1/b$ . As we shall later see,  $b$  plays the role of magnetic flux in a 2D tight-binding model subject to an external magnetic field (the superspace model). Both intracell and intercell hoppings are varied by the cosine term equivalently within each unit cell. In other words, within each unit cell, the hopping modulation occurs only due to the difference in the strength parameters  $\Delta_1$  and  $\Delta_2$ . The parameter  $\delta$  represents an overall shift in

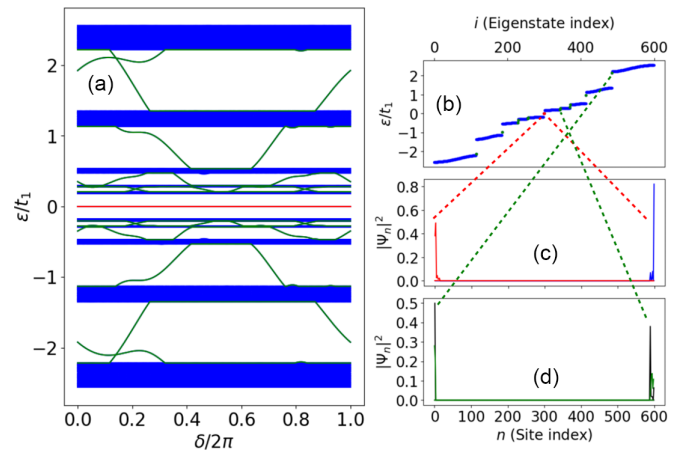


FIG. 3. (a) Spectra of the cAA model as a function of the phasonic degree of freedom or modulation shift  $\delta$  with parameters  $t_1 = t_2 = \Delta_1 = 1$  and  $\Delta_2 = 0.5$  and a periodicity of  $\tau \equiv (1 + \sqrt{5})/2$ . Bulk bands are clearly observed with their position remaining unchanged as  $\delta$  is varied. Due to the presence of chiral symmetry a topological insulator phase is verified, with persistent topological zero-energy mode across all  $\delta$  values, as well as edge states located in the gaps. (b) Spectrum of a physical realization of the cAA model, corresponding to the phasonic parameter  $\delta = 0$ . The doubly degenerate zero-energy modes are highlighted in red, while the additional visible edge states are marked in green. Notably, not all finite-energy edge states are visible for a particular  $\delta$ . (c) Wave functions for the zero modes highlighted in red in panel (b). Red and blue colors indicate the *A* and *B* sublattice respectively. The relative strength of each edge mode is found to change depending on the choice of  $\delta$ . (d) Wave functions for the modes highlighted in green in panel (b). Unlike the zero-energy edge states, which localize at one or the other sublattice, finite-energy edge modes have a finite probability of existing in both sublattices, despite the different overlapping profiles within each one as seen with the green and black lines denoting the wave function at the *A* and *B* sublattice respectively.

the hopping modulation, constituting a phasonic degree of freedom. We define the chiral Aubry-André (cAA) model as  $H_{\text{CAA}}(\delta) \equiv H_{\text{SSH}} + H_{\text{odAA}}(\delta)$ .

The spectral properties of the cAA model exhibit the remarkable complexity expected from a quasicrystal: In the case where the hopping modulation is commensurate with the lattice spacing, with  $L = p/q \in \mathbb{Q}$ , the spectrum comprises  $q$  well-defined bands, and the Brillouin zone becomes, itself,  $q$  periodic. However, in the quasicrystalline limit where  $L \notin \mathbb{Q}$ , the spectrum transforms into a Cantor set, lacking a well-defined band structure. Nevertheless, in this latter case, the spectrum separates into regions characterized by a dense arrangement of states in the thermodynamic limit, called quasibands. Figure 3 depicts a chain with  $N = 600$  lattice sites, showcasing the effect incommensurate hopping modulations. In particular, for this figure, we take the periodicity to be equal to the golden ratio  $L = \tau$ . Note that to assign a numerical value to an irrational periodicity, one can consider a rational approximant to such value  $p/q$  such that  $q$  is much larger than the number of lattice sites  $q \gg N$ . For the case with  $N = 600$ , we consider  $\tau = 1346269/832040$ , which is the ratio of the 31st and 30th Fibonacci numbers. In all subsequent cases

where irrational values of  $b$  are considered, its value is chosen as above. The effect of considering a finite size chain in real space is postponed for Sec. IV, when we explore the genesis of Dirac cones and the crossover from periodic to quasiperiodic modulation. For now, note that this figure clearly illustrates the appearance of quasibands, but also the existence of in-gap edge states in the cAA model. The edge states connect between quasibands as the phasonic degree of freedom is shifted, as demonstrated in Fig. 3(a).

From the 1D point of view, this points to the ability of sending zero-energy edge states into the bulk by manipulating the phasonic degree of freedom  $\delta$ . Indeed, one important feature to consider, is that a physical realization of the cAA model comprises a single value of  $\delta$  [see panel (b)]. One should therefore not interpret our figures such as panel (a) as physical ribbons of material. Rather, only from the superspace interpretation of the phasonic degree of freedom  $\delta$  as a momentum along a synthetic direction can one map the 1D chain into a ribbon like structure with periodic boundary conditions along the synthetic direction. The physically accessible spectrum is, in reality, only a slice of the ribbon spectrum at a fixed value of  $\delta$ . This way, a realization of the 2D superspace model actually corresponds to many possible physical realizations of the cAA model, each related to each other by translations in the phason  $\delta$ . Finally, a comment is in order, with regards to the shape of the envelope of the zero energy edge modes. In the standard SSH model, they decay exponentially in the A and B sublattice for the left and right edges respectively, however, this exponential decay is not universal. In the Appendix B an analogy between zig-zag graphene ribbons and the SSH model via dimensional reduction is provided. For the case of these zig-zag ribbons, it is well known that presence of defects can induce different envelopes for the edge-state wave functions [39]. Here also the presence of quasiperiodic disorder can induce changes in the modulation of the edge-state wave functions, including via changes in  $\delta$ .

### III. GENESIS OF DIRAC CONES IN THE VANISHING FIELD LIMIT

To shed some light on the origin of the topological origin of the edge-state structure and further spectral properties of the cAA model, as well as set up the necessary tools for the topological analysis of the model. We now focus on what we call a vanishing field (small  $b$ ) limit, or equivalently on a large periodicity (large  $L$ ) limit. To order  $\mathcal{O}(b)$ , the field dependence drops out from the Hamiltonian; however, we can nevertheless consider its extension to a superspace model. It is worth noting that this approximation must be performed carefully, but it remains valid so long as the periodicity is much larger than the total length of the system  $N$ , i.e., this approximation can be performed, for  $b = p/q$ , only in the limit  $pN \ll q$ . The case of an incommensurate periodicity can be recovered trivially by considering successive approximants  $p/q$  to the desired value of  $b$ . The advantage of this vanishing field treatment is that many of the model's properties can be analytically computed in this limit, and intuition can be gained and later utilized for the generic case of finite and possibly large fields. For vanishing fields, the Hamiltonian reads, in a real space

description

$$H_{2D} = - \sum_{i,j} t_1 a_{i,j}^\dagger b_{i,j} + \frac{\Delta_1}{2} a_{i,j}^\dagger b_{i,j+1} + \text{H.c.} \\ - \sum_{i,j} t_1 b_{i,j}^\dagger a_{i+1,j} + \frac{\Delta_2}{2} b_{i,j}^\dagger a_{i+1,j+1} + \text{H.c.}, \quad (3)$$

where we have switch from the variable  $n$  indexing physical state sites to the pair  $(i, j)$ , where  $j$  represents the lattice index along the synthetic dimension. The change from  $n$  to  $i$  is merely a notational convention to place both directions in the same footing. One of the advantages of this limit is that we can analyze the case where we have an infinitely long chain with periodic boundary conditions, such that it becomes possible to construct Brillouin zone parameterized by momenta along the synthetic direction  $\delta \in [0, 2\pi[$  and the physical direction  $k \in [0, 2\pi[$ . Denoting  $\mathbf{k} = (k, \delta)$  also allows for a representation of the superspace Hamiltonian in the form of a matrix  $H_{2D}(\mathbf{k})$  as  $H_{2D} = \sum_{\mathbf{k}} \Psi_{\mathbf{k}}^\dagger H_{2D}(\mathbf{k}) \Psi_{\mathbf{k}}$ , where  $\Psi_{\mathbf{k}}^\dagger = (a_{\mathbf{k}}^\dagger, b_{\mathbf{k}}^\dagger)$ , and with  $H_{2D}(\mathbf{k})$  explicitly given by (see Appendix A for details)

$$H_{2D}(\mathbf{k}) = - [t_1 + \Delta_1 \cos \delta + (t_2 + \Delta_2 \cos \delta) \cos k] \sigma_x \\ - [(t_2 + \Delta_2 \cos \delta) \sin k] \sigma_y. \quad (4)$$

This shows that the vanishing field Hamiltonian can be realized in the form of a Dirac model, at the cost of the  $\sigma_x$  and  $\sigma_y$  Pauli matrices, but does not include a  $\sigma_z$ . This is to be expected, once again, due to the presence of chiral symmetry. Indeed, we see that coupling between replicas of the model along  $j$  preserves the fact that hopping can occur only between A and B sublattices or vice versa. Again, if one were to consider an AA type on-site modulation, this would induce couplings among different sites of the A sublattice and of the B sublattice, thus breaking the chiral symmetry of the 1D chain. Now, for all quasicrystalline systems, a treatment using synthetic dimensions is possible; however, chiral symmetry makes this model extremely interesting, since the superspace model becomes a semimetal with topological properties.

We say that it is a semimetal since the cAA model can host at most four distinct massless Dirac cones in this vanishing field limit, the positions of which are not restricted to any high-symmetry points of the Brillouin zone, but rather can wander around certain lines within it, depending on the parameter space spanned by  $t_1, t_2, \Delta_1$ , and  $\Delta_2$ . To show that this is the case, given Eq. (4), it is simple to diagonalize the Hamiltonian and find the energy spectrum  $\varepsilon(k, \delta)$ . Finding the points at which massless Dirac cones occur, then becomes a matter of analytically solving  $\varepsilon(k, \delta) = 0$ , which yields the solutions

$$\delta_D(k) = \pm \arccos \left( \frac{e^{ik} t_1 + t_2}{e^{ik} \Delta_1 + \Delta_2} \right) \cap \mathbb{R}, \\ \delta_D(k) = \pm \arccos \left( \frac{t_1 + e^{ik} t_2}{\Delta_1 + e^{ik} \Delta_2} \right) \cap \mathbb{R}. \quad (5)$$

We have explicitly included an intersection with the real numbers to make explicit the fact that the  $\arccos(z)$  function may have solutions corresponding to complex numbers; however, we retain only real solutions, corresponding to real momenta  $\delta$ . Additionally, near the location of these Dirac

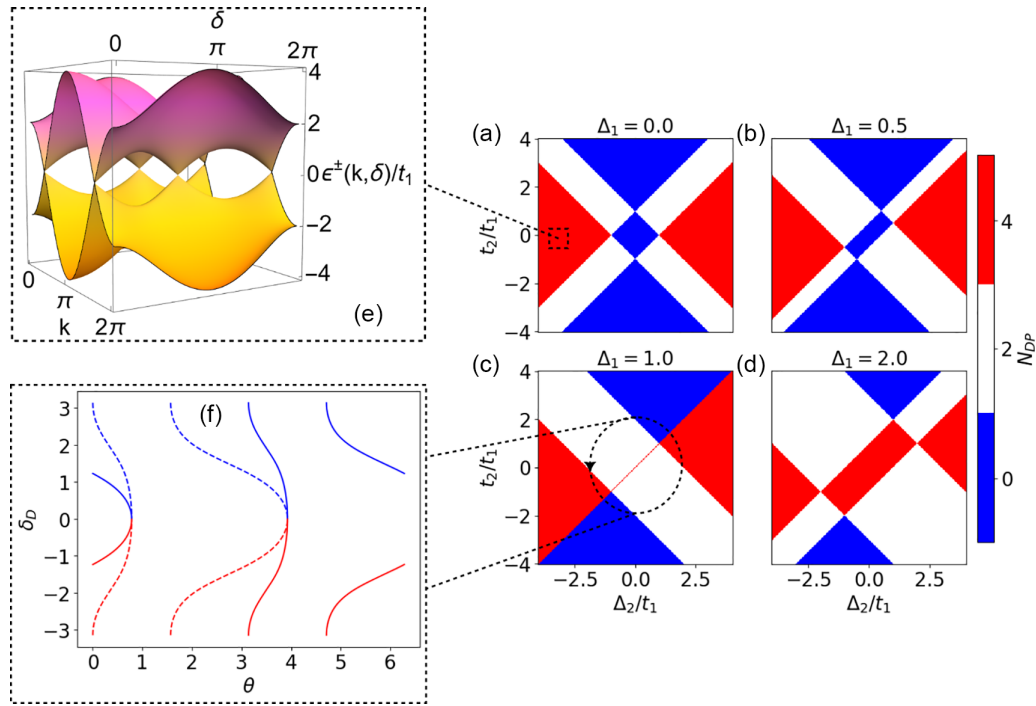


FIG. 4. [(a)–(d)] Phase diagrams for the number of Dirac points  $N_{DP}$  as a function of the models parameters measured relative to  $t_1$ . In (c), the line  $\Delta_2 = t_2$  corresponds to a situation where the bands touch not only at specific points, but rather along a full line, at  $\delta = 0$  and for any value of  $k$ , such that the model actually is in a topological nodal line semimetal phase. (e) Band structure of the cAA model showcasing the existence of 4 massless Dirac cones occurring for the parameters  $t_1 = 1$ ,  $t_2 = 0$ ,  $\Delta_1 = 0$ ,  $\Delta_2 = -3$ . (f) Trajectories of the Dirac cones for  $k = 0$  (continuous lines) and  $k = \pi$  (dashed lines), as a circle is traversed in the parameter space as indicated in (c). Note that Dirac cones always come in pairs located one above (blue) and one below (red) the line  $\delta = 0$ . The hopping amplitudes are parameterized with  $\Delta_2 = 2 \cos \theta$  and  $t_2 = 2 \sin \theta$ , and  $\theta$  is varied from 0 to  $2\pi$ . Several Dirac cone mergers are observed as  $\theta$  is varied both at  $k = 0$  and  $k = \pi$ .

cones, the energy dispersion can be extracted analytically. If we expand the momentum radially near  $\mathbf{K}_D = (k, \delta_D(k))$  as  $\mathbf{q} = \mathbf{K}_D + q(\cos \theta, \sin \theta)$  with  $q = \sqrt{k^2 + \delta^2}$ , we can write down a linearized form of the dispersion. In particular, if we consider the terms

$$\eta_1 = (t_2 \Delta_1 - t_1 \Delta_2) / (\Delta_1 - \Delta_2)^2, \quad (6)$$

$$\eta_2 = (t_2 \Delta_1 - t_1 \Delta_2) / (\Delta_1 + \Delta_2)^2, \quad (7)$$

$$\xi_1 = (t_1 - t_2 + \Delta_1 - \Delta_2)(t_2 - t_1 + \Delta_1 - \Delta_2), \quad (8)$$

$$\xi_2 = (\Delta_1 + \Delta_2 - t_1 - t_2)(t_1 + t_2 + \Delta_1 + \Delta_2), \quad (9)$$

then the linearized dispersion around the Dirac cones reads

$$\varepsilon_1 = \pm q \sqrt{\eta_1 \cos^2 \theta + \xi_1 \sin^2 \theta}, \quad (10)$$

$$\varepsilon_2 = \pm q \sqrt{\eta_2 \cos^2 \theta + \xi_2 \sin^2 \theta}. \quad (11)$$

Evidently, these expressions hold only when the massless Dirac cones exist, i.e., when there exists a solution to Eq. (5). As can be seen from (10) and (11), these Dirac cones are generically anisotropic since  $\eta_i \neq \xi_i$ . By probing the parameter space of the model, we identify five possible phases for the superspace model: Phase (i) corresponds to a semimetal phase with two massless Dirac cones at  $k = 0$ ; Phase (ii) corresponds to a similar semimetal phase with two massless Dirac cones at  $k = \pi$ ; Phase (iii) is an insulating phase, with

no massless Dirac cones; Phase (iv) is a semimetallic phase, with four massless Dirac cones, two of which are located at  $k = 0$  and another two at  $k = \pi$ . For all phases where Dirac cones are visible, they are arranged symmetrically around  $\delta = 0$ . Phase transitions between these four phases occur due to merging and subsequent lifting of the Dirac cones as the parameters of the model are tuned. These mergings can occur either at the edge ( $\delta = \pm\pi$ ) or the center ( $\delta = 0$ ) of the Brillouin zone along  $\delta$ . The final phase (v) occurs only for very specific choices of the parameters, where at the critical point of a simultaneous fusion of Dirac cones at  $k = 0$  and  $k = \pi$  a nodal line semimetal phase is observed, with the two bands touching along all values of  $k$  and  $\delta = 0$ .

We illustrate the wandering, merging, and subsequent appearance or disappearance of massless Dirac cones in Fig. 4(f) for a specific choice of parameters. Different phase diagrams can also be drawn by picking three parameters with varying strength relative to a fourth one. For instance, we can vary  $\Delta_2/t_1$  and  $t_2/t_1$  while choosing a few different values of  $\Delta_1/t_1$ . For values of  $\Delta_1/t_1 = 0, 0.5, 1, 2$ , we plot some phase diagrams in Fig. 4. Remarkably, the number of pairs of Dirac cones in this model can be shown to be related to the topological properties of the 1D model. To see why this is the case, we can think of the momentum  $\delta$  as a tunable parameter, which is likely indeed be the case for any realistic implementation of the cAA model. If this is so, a massless Dirac cone occurring in the model corresponds to the band gap closing when  $\mathbf{K}_D = (k, \delta_D(k))$  is approached. For this reason,

it becomes very useful to consider a winding number as a function of  $\delta$ , such that each particular physical implementation of the cAA model has its own  $W(\delta)$ . Due to the presence of chiral symmetry, the Hamiltonian matrix can be brought into the form

$$H(\mathbf{k}) = \begin{bmatrix} 0 & q(\mathbf{k}) \\ q^*(\mathbf{k}) & 0 \end{bmatrix}, \quad (12)$$

and the Winding number can be defined as

$$W(\delta) = \frac{1}{2\pi i} \int_0^{2\pi} dk \frac{\partial}{\partial k} \log q(k, \delta). \quad (13)$$

Another reason we may be interested in such a quantity, besides the fact that it signals the presence or absence of a zero-energy edge mode at each  $\delta$  is that transition points between the two topological phases are also of physical relevance. These are precisely the set of points at which massless Dirac cones occur. An analytical computation of the winding number from Eq. (13), results in

$$W(\delta) = \Theta(|t_1 + \Delta_1 \cos \delta| - |t_2 + \Delta_2 \cos \delta|), \quad (14)$$

as could be anticipated from the topological properties of a standard SSH model. Here,  $\Theta(x)$  represents the Heaviside step function of  $x$ .

Now, the parity number of pairs of Dirac points,  $N_{2DP} \bmod 2$ , can be counted by looking at whether the winding number is the same when  $\delta = 0$  and when  $\delta = \pi$ . One considers, in particular, the winding number at  $\delta = 0$ , since the Dirac cones always come in pairs, due to the Fermion doubling theorem [40,41], and furthermore are always located symmetrically around this point. Hence, we know that if the Winding number is the same at  $\delta = 0$  and  $\delta = \pi$  then it must have changed an even number of times between these two values of  $\delta$ , leading to an even number of pairs of Dirac points. Otherwise, if it is not the same, it must have changed an odd amount of times, leading to an odd number of pairs of Dirac points. Hence, we have the simple formula

$$N_{2DP} \bmod 2 = |W(\pi) - W(0)|. \quad (15)$$

This quantity already provides some information regarding the presence or absence of massless Dirac cones, but the total number of Dirac cones  $N_{DP}$  in the Brillouin zone cannot be counted in this manner. One simple way to augment this result is to sum over changes in  $W(\delta)$  along the entire range of  $\delta$ , instead of considering only  $\delta = 0$  and  $\delta = \pi$ . In particular, since the winding number varies as a series of step-functions, taking the derivative of  $W(\delta)$  along  $\delta$  will yield a series of Dirac-delta functions. If these delta functions are integrated over, each one contributes with unity, and thus we can count the number of times such changes occur, and thus we have

$$N_{DP} = \int_0^{2\pi} d\delta \left| \frac{\partial}{\partial \delta} W(\delta) \right|. \quad (16)$$

These considerations can also be applied to ribbons of familiar 2D materials such as graphene, and we illustrate some analogies between the cAA model and zig-zag ribbons of graphene in Appendix B, providing a topological description of the emergence of zero-energy edge states in these configurations.

For now, in order to demonstrate the practical application of the aforementioned formula (16), we have employed it to compute phase diagrams for the model, as depicted in Figs. 4(a)–4(d). The diagrams clearly indicate that the count of Dirac cones consistently falls into one of three possibilities: 0, 2, or 4, regardless of the model's parameters. Indeed, these diagrams, along with Fig. 4(f) make it clear that it becomes possible to induce a transition from a state characterized by the presence of an energy band gap to one featuring a gapless state with Dirac cones. The genesis of Dirac cones will have observable effects, even when the system is projected down to physical space, particularly concerning edge states in the 1D physical model when the AA hopping modulation is increased. A detailed exploration of this phenomena is presented in the following section.

#### IV. COEXISTENCE OF 1D AND 2D TOPOLOGY AT FINITE FIELDS

To study the effects of a magnetic field on the superspace 2D model in more detail, i.e., if one moves away from the limit of slowly varying hopping modulations for the 1D physical system, a number of possible approaches present themselves, but none is as clean as the analytic treatment provided in the previous section. The added difficulty stems from the explicit breaking of translational symmetry of the 1D model. The standard toolkit for the IQHE could be applied by analyzing the  $L \in \mathbb{Q}$  case and the notion of the magnetic translation group; however, a simple analysis of an incommensurate modulation remains, nonetheless analytically out of reach. For this reason, we implement a numerical method based on recently proposed topological markers for Dirac models and quasicrystals, which is capable of handling the problem in full. Two topological markers become relevant for our discussion: The first is a winding number marker and the second is a quasicrystal Chern marker. Since the cAA is a Dirac model, both are “different dimensional shadows” of the same invariant known as the wrapping number as pointed out by von Gersdorff and Chen [34]; however, we take different approaches to their calculation, and use the method of Chen [35] only for the winding number marker. This approach is based on the construction of a 1D universal topological operator of the form

$$\hat{C}_{1D}(\delta) = N_D \mathcal{W}[Q(\delta)\hat{x}P(\delta) + P(\delta)\hat{x}Q(\delta)], \quad (17)$$

where generically  $N_D$  is a normalization factor, here simply unity, and  $\mathcal{W}$  is a Pauli matrix, which remains unused in the Dirac model Hamiltonian: the  $\sigma_z$  Pauli matrix.  $P$  and  $Q$  are projectors into occupied and unoccupied states,

$$P = \sum_{E < E_F} |n_E\rangle \langle n_E|, \quad (18)$$

$$Q = \mathbb{1} - P. \quad (19)$$

For clarity, we make here the assumption that the cAA model is fermionic, which on the one hand makes the concept of occupation of bands well defined, and on the other hand, sets the IQHE interpretation of the superspace description on firmer ground, since this effect is often considered to be reserved for fermionic models. Although this is not really the case, with Hofstadter models having been obtained for bosonic systems

as well [42], we nevertheless stick to the analysis of fermionic systems for clarity. Furthermore, expected implementations in cold-atom systems or spin systems rely on fermions (electrons and Jordan-Wigner Fermions respectively). The use of fermions allows for the consideration of a Fermi energy  $E_F$ , and for all future discussion and computations presented in this paper, we will focus on neutral systems, with  $E_F = 0$ . Finally, in Eq. (17),  $\hat{x}$  is the position operator, which, as stated in Sec. II, is assumed to have the same eigenvalue for states localized within each of the two sites within the unit cell of the cAA model. The local winding number marker at a given position  $x$  of the model is then generically computed as the diagonal matrix element of the topological operator

$$W(x, \delta) = \langle x | \hat{C}_{1D}(\delta) | x \rangle = \sum_{\sigma} \langle x, \sigma | \hat{C}_{1D}(\delta) | x, \sigma \rangle, \quad (20)$$

where  $\sigma$  indicates, generically, all internal degrees of freedom of the model. In the BDI symmetry class, for the SSH model,  $\sigma = A, B$  are simply the two pseudospin projections (sublattice types). Indeed, the Hamiltonian  $H_{\text{odAA}}(\delta)$  [Eq. (2)] is here interpreted simply as a disorder term, and hence, even in the case where the unit cell becomes effectively larger due to the periodicity of modulation, we always retain the summation to be over the two sites corresponding to the unit cells of the model described by  $H_{\text{SHH}}$  [Eq. (1)]. When we consider a finite cAA chain, this winding number marker is expected to coincide with the winding number topological invariant deep in the bulk, and decay near its boundaries. For this reason, due to the presence of spatial disorder, and for numerical stability, an averaging over a finite region  $\mathcal{R}$  of size  $N_{\mathcal{R}}$  deep in the bulk is performed, so that the behavior at the edges is avoided. In the end, the winding number invariant can be computed as

$$W(\delta) = \frac{1}{N_{\mathcal{R}}} \text{tr}_{\mathcal{R}}(\hat{C}_{1D}(\delta)) = \frac{1}{N_{\mathcal{R}}} \sum_{x \in \mathcal{R}} W(x, \delta). \quad (21)$$

Note that, in the cAA model, this topological invariant is computed purely from a single slice of the superspace model at a fixed  $\delta$ , and, once again, the role played by the odAA term is merely one of introducing spatial disorder. On the other hand, to access the Chern number, the phasonic degree of freedom must come into play, and all slices of fixed  $\delta$  become relevant. The use of a 2D universal topological marker as proposed by Chen, however, would be unwise, because the cAA model is actually only disordered in the physical 1D space. A 2D universal topological marker is much better suited to the analysis of disordered 2D lattices, and thus, as an alternative, a recently proposed method originally due to Sykes and Barnett [36] is therefore employed. This method is particularly suited for handling models like the AA models or other 1D quasicrystals, and its underlying insight is to interpret the phasonic degree of freedom  $\delta$  as a function of time,  $\delta(t) = 2\pi t/T$ , which enables us to think of the 1D chain as undergoing an adiabatic and  $T$ -periodic evolution. This interpretation is made physical in systems exhibiting the so-called Thouless or topological pump, which is a quantized pump of charge from one edge of a 1D chain to the other over the course of a period  $T$  [43]. The topological pump can be directly observed when a 1D crystal is periodically driven by an external field. The charge pump is topologically protected

by what is effectively the 2D Chern number for the superspace model.

By interpreting the phasonic degree of freedom as proportional to time, regardless of its actual nature (in previous discussions we have assumed that  $\delta$  is a fixed parameter), we can compute the topological pump due to an effective adiabatic Hamiltonian [36], which can be shown to be

$$h(t) = i \left[ \frac{\partial P(t)}{\partial t}, P(t) \right], \quad (22)$$

This effective Hamiltonian induces an effective adiabatic evolution operator  $U(t) = \exp(iht)$ , and  $P(t) = U^\dagger(t)PU(t)$  is the projector onto occupied states at time  $t$ . The local topological quasicrystal marker [36] can, in turn, be defined as the expectation value of a topological operator  $\hat{M}_{1Q}(\delta)$ , as in

$$\begin{aligned} M_{1Q}(x, \delta) &= \langle x | \hat{M}_{1Q}(\delta) | x \rangle \\ &\equiv \langle x | P(t)U^\dagger(t)\hat{x}U(t)P(t) | x \rangle. \end{aligned} \quad (23)$$

Much like in the case of the winding number marker, averaging over a region  $\mathcal{R}$  deep in the bulk of the quasicrystal is necessary, and we compute  $M_{1Q}(t) = \text{tr}_{\mathcal{R}}(\hat{M}_{1Q}(t))/L_{\mathcal{R}}$ . This quantity measures the location of the so-called Wannier center at time  $t$ , and, as described by the modern theory of polarization [44,45] (or the Thouless pump). Then, the difference in position of the Wannier center at time  $t_0$  and  $t_0 + T$  gives the polarization change or charge transfer over the course of a period of the driving. This charge transfer is nothing but the 2D Chern number characterizing the superspace model, and hence, setting  $t_0 = 0$  for simplicity, at which point  $U(0) = 1$ , the invariant is [36]

$$C = M_{1Q}(T) - M_{1Q}(0). \quad (24)$$

Armed with these two topological invariants,  $C$  and  $W(\delta)$ , and the respective methods of computation in real space, we are primed to characterize the topology of the cAA model. Note that the winding number characterizes the topology of the model for each value of  $\delta$ , and hence, for a computation of  $C$  one may actually be integrating over topological phases with  $W(\delta) = 0$  and  $W(\delta) = 1$ , which is another pointer to the subtle nature of how  $C$  characterizes the 1D phase, despite being an invariant, which finds a natural setting in 2D.

A simple way to illustrate the power of the quasicrystal topological marker is to compute the Chern number for the cAA model as a function of the modulation periodicity and Fermi energy of the model. For each value of  $b$  and  $E_F$ , we compute  $M_{1Q}(0) = \text{tr}_{\mathcal{R}}(P(0)\hat{x}U(t)P(0))/N_{\mathcal{R}}$ , and afterwards compute the time evolved projection operator  $P(t)$  by slicing the period  $T$  into slices of size  $\Delta t$ .

A  $U(t + \Delta t) \approx \exp(-ih(t)\Delta t)U(t)$  at each successive interval, one can calculate the Wannier center  $M_{1Q}(t)$ , and iterating this procedure over one period, we can compute  $C$  using (24). Computing  $C$  for each value of  $b$  and  $E_F$  reveals a striking illustration of a colored Hofstadter butterfly [18]. Two examples of these colored Hofstadter butterflies, for topological insulating and topological semimetal phases are provided in Fig. 5.

Furthermore, the winding number topological marker clearly counts, for each value  $\delta$ , the presence or absence of the zero-energy edge mode even when  $b$  is a finite quantity.



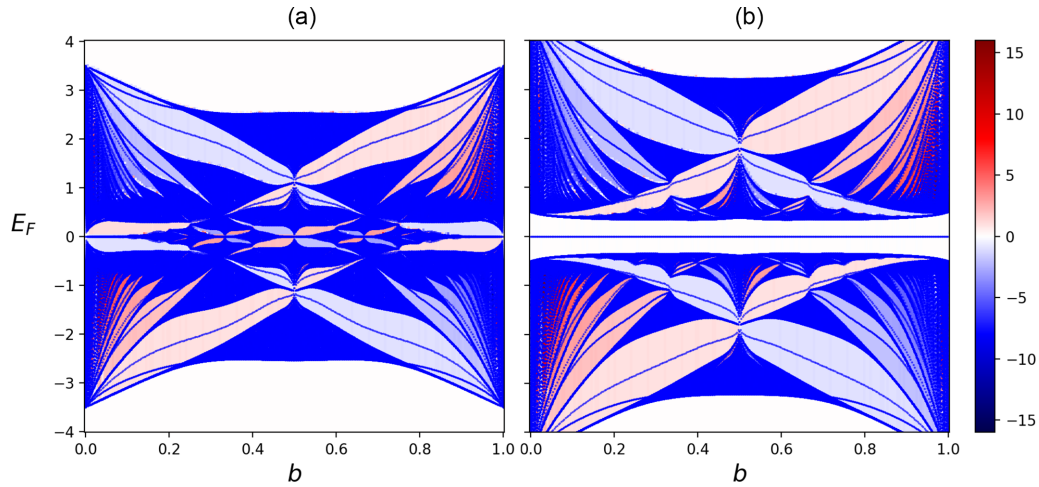


FIG. 5. Chern number calculated from the topological marker as a function of the periodicity  $b$  and the Fermi energy  $E_F$ . The resulting plots produce a fractal image corresponding to a colored Hofstadter butterfly, where the coloring indicates the value of the Chern number, and the thick blue lines indicate the energy levels. (a) Semimetal phase, with parameters  $t_1 = t_2 = \Delta_1 = 1$  and  $\Delta_2 = 1.5$ . At charge neutrality, there is no trivial Chern phase, and the Chern number jumps from  $C = -1$  to  $C = 1$  or vice versa. This is analogous to the case of the half-integer quantum Hall effect in graphene. (b) Insulating phase with  $t_1 = t_2 = \Delta_1 = 1$  and  $\Delta_2 = 0.5$ . At neutrality, there exists a trivial Chern phase. This is analogous to the integer quantum Hall effect observed, for instance a square lattice material. The presence of the zero-energy modes in panel (b) is indicative of the presence of nontrivial 1D topology, accounted for by a winding number  $W(\delta) = 1$ . Although this is not so clearly visible in panel (a), these states can also exist at zero energy for semimetal phases at certain values of  $\delta$ , but are generically not present for all values of modulation shift.

In particular, this enables us to count the number of Dirac cones using Eq. (16), in exact analogy to the approach we took for vanishing fields. A band touching point induces an abrupt change in  $W(\delta)$ , even when the modulation periodicity is irrational.

Let us consider the example case where  $b$  is given by successive rational approximations to the inverse golden ratio  $1/\tau$ . Numerically, as  $1/\tau$  is approached, the method becomes more costly due to the necessity of a large sampling of points along  $\delta$ , but nonetheless we can illustrate the behavior of convergence to an irrational periodicity by producing several plots of phase diagrams depending on the model's parameters. These are presented in Figs. 6(a)–6(d). We observe that, as the irrational limit is approached, the number of massless Dirac cones increases. In particular for finite and rational values  $1/b = p/q$  of the field, the number of massless Dirac cones appears to always be given by  $0, 2q$  or  $4q$ .

For infinite chains, we would expect this behavior to continue *ad infinitum*, with the bands becoming perfectly flat and gapless in the limit of infinite unit cell and system size, as the Dirac cones become denser in the Brillouin zone. Furthermore, as the periodicity is brought closer and closer to an irrational value, or in other words, if we focus on the large  $q$  limit and keep  $p/q$  finite, the system's physical size can also become relevant, leading to a departure from the seemingly observed trend of the number of  $0, 2q$ , or  $4q$  Dirac cones, instead stabilizing at some finite value. This is observed in Fig. 6(e).

The crux of this discussion is that the genesis of Dirac cones in the superspace model of the cAA is found to be mappable to changes in a topological invariant as the phasonic degree of freedom is spanned over. We find this to be an interesting result in and of itself, as tuning  $\delta$  could

be a useful knob for tuning physical properties such as the conductivity at half-filling.

Besides this, we can now use these topological markers to explicitly showcase the coexistence of 1D and 2D topology in the cAA model, by computing both invariants for some parameter values. This calculation is performed in Fig. 7, where we find phases of type  $(C, W) = (0, 1), (\pm 1, 1), (\pm 2, 1), (\pm 3, 1)$ , and  $(\pm 1, 0)$ . As can be clearly seen in this figure, the Chern number counts the number of in-gap edge states for all possible values of  $\delta$ . A point, which cannot go without mentioning is that even though a Chern number exists and this bulk-boundary correspondence is verified in the superspace model, the number of 1D edge modes, which occur in a given energy gap of any particular physical realization of the cAA model is not in direct correspondence with this Chern number. The 2D topological invariant merely points to how many edge states *can* occur at the edge of the 1D model if the odAA modulation is shifted relative to the lattice.

Nevertheless, for a physical realization of the cAA model, and for a Fermi energy  $E_F$  located within a gap above the zero energy  $\varepsilon = 0$ , it is clear that both  $W$  and  $C$  are necessary quantities to characterize the topology of the model, as zero-energy edge states will be measured depending on  $W(\delta)$ , and finite-energy edge states will be visible depending on both  $C$  and  $\delta$ .

This coexistence can then be manifest in many different ways, depending on whether the modulation is commensurate or incommensurate with the lattice, as well as depending on the periodicity itself. Figure 7 showcases both commensurate and incommensurate modulations, yielding in the latter case a zero-energy edge mode visible for all  $\delta$ , and in the former a zero-energy edge mode, which wanders into the bulk for

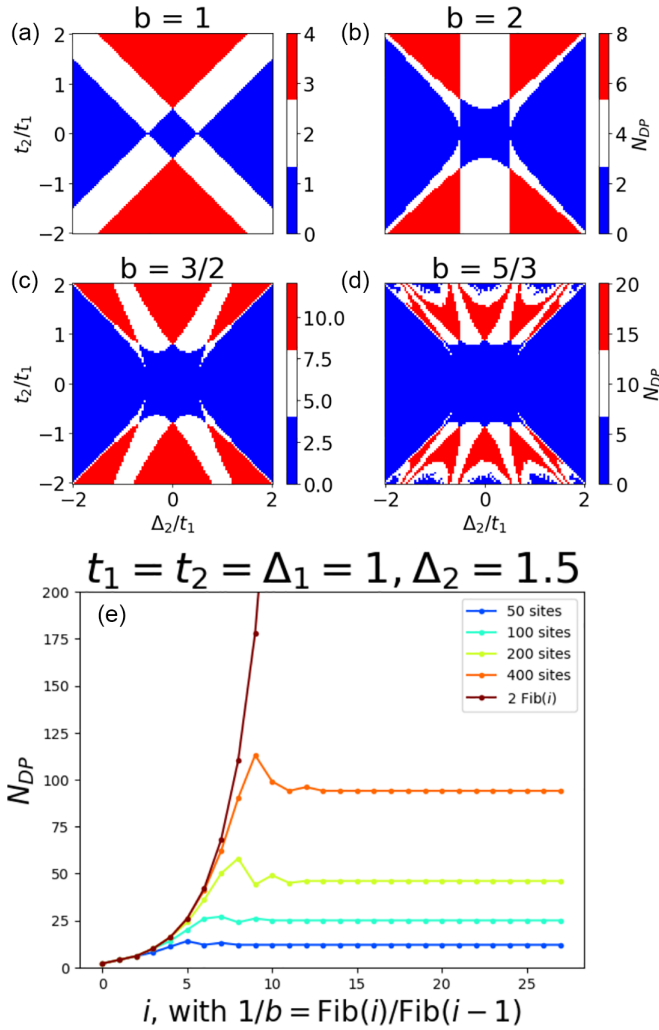


FIG. 6. [(a)–(d)] Number of Dirac nodes calculated from our method relying on the 1D winding number for finite  $b$  and fixed  $\Delta_1 = 0$ . For each of the phase diagrams, successive approximants to the golden ratio  $\tau = (1 + \sqrt{5})/2$  are utilized as the inverse field. Explicitly, we use  $b = 1, 2, 3/2$ , and  $5/3$ . (e) Growth of the number of nodes as better approximants are utilized. The colored curves correspond to different system sizes. Increasing this size shifts the point at which the number of Dirac nodes stabilizes. We compare the curves, which give the number of Dirac cones with twice the  $i$ th Fibonacci number, i.e. with  $2\text{Fib}(i) = 2q$ . We see that the behavior of the curves saturates near the size of the system, i.e. for  $2q \sim N$ , and begins deviating from the expected behavior slightly earlier, when finite-size effects come into play and already a few unit cells become comparable with the system size.

some values of  $\delta$ . As can be seen from this figure, the position, number and distribution of gaps, as well as edge states within each gap, depends on the model’s parameters, such as the relative magnitudes of the  $J_i$ s and  $\Delta_i$ s. However, the evaluation of  $W(\delta)$  and  $C$  is always possible, and provides a signature or probe to the appearance of edge modes.

Finally, it is worth mentioning that that intuition about this model can be gained by drawing an analogy to the well-understood model of the Half-integer quantum Hall effect (HIQHE) in graphene. For instance, if we pick  $1/b = 1/2001$ ,

by computing the wave function of edge states for certain values of  $\delta$ , we see how, much like in the case of zig-zag graphene ribbons, a zero-energy edge mode can turn into a Landau-level edge state given the presence of Dirac cones in the 2D model. Additionally, the square root dispersion of the Landau levels, characteristic to the HIQHE, also becomes clearly observable. The dispersion in the presence of finite and small  $b$  is showcased in Fig. 8, together with the useful winding number invariant, which is unity while the model hosts zero energy modes, and becomes zero after the degeneracy is lifted by shifting the modulation. The possibility of changing the edge localization of the wave function as  $\delta$  is shifted is also illustrated in Fig. 9.

The difference relative to the 2D case of graphene, is, of course, the fact that  $\delta$  is a fixed parameter for a physical realization of the cAA model, and hence the existence of edge modes of the 1D model are also fixed, up to physical changes in  $\delta$ .

## V. CONCLUSIONS AND OUTLOOK

In this paper, we have introduced and studied the properties of a chiral symmetric SSH-type model perturbed by an off-diagonal Aubry-André (odAA) modulation, resulting in what we call the cAA model. The main result of the paper is the explicit demonstration that topological invariants characteristic of different dimensionalities can coexist in a physical way in a tight-binding purely one dimensional chain. We believe that this result paves the way for a series of topologically nontrivial models with admixtures of different topological invariants, thus increasing the tuneability and application range of topological systems. Our idea is that by applying an incommensurate potential to a system, which already hosts some sort of topological invariant due to the presence of a symmetry, the topology of the model can be enhanced via the generation of synthetic dimensions with topologically nontrivial degrees of freedom. This admixture of topological invariants will then be manifest in the original system by the possibility of introducing edge states of different character, such as the zero-energy edge modes, and Landau levels, as observed here in the cAA model.

To showcase this, we first analytically explored a limit of large modulation periodicity of the cAA model, corresponding to what we call the “vanishing-field limit”. Here, we have found many interesting properties, such as the existence of a quantized winding number and the presence of Dirac cones when a 2D crystalline superspace model is constructed. In addition, we have provided a way to compute the number of massless Dirac cones solely from the winding number, counting the amount of times its value is changed as the AA modulation is shifted relative to the lattice. We have found that 0, 2, or 4 cones appear in the vanishing-field limit, located at variable positions along certain lines in the superspace Brillouin zone. This position depends on the relative strengths of hoppings and modulations.

Then, we extended this methodology to the case of smaller odAA modulation periodicity, by making use of topological markers. For periodicities commensurate with the lattice and  $1/b = p/q$ , we have found the number of massless Dirac cones in the superspace description is 0,  $2q$ , or  $4q$ , for small

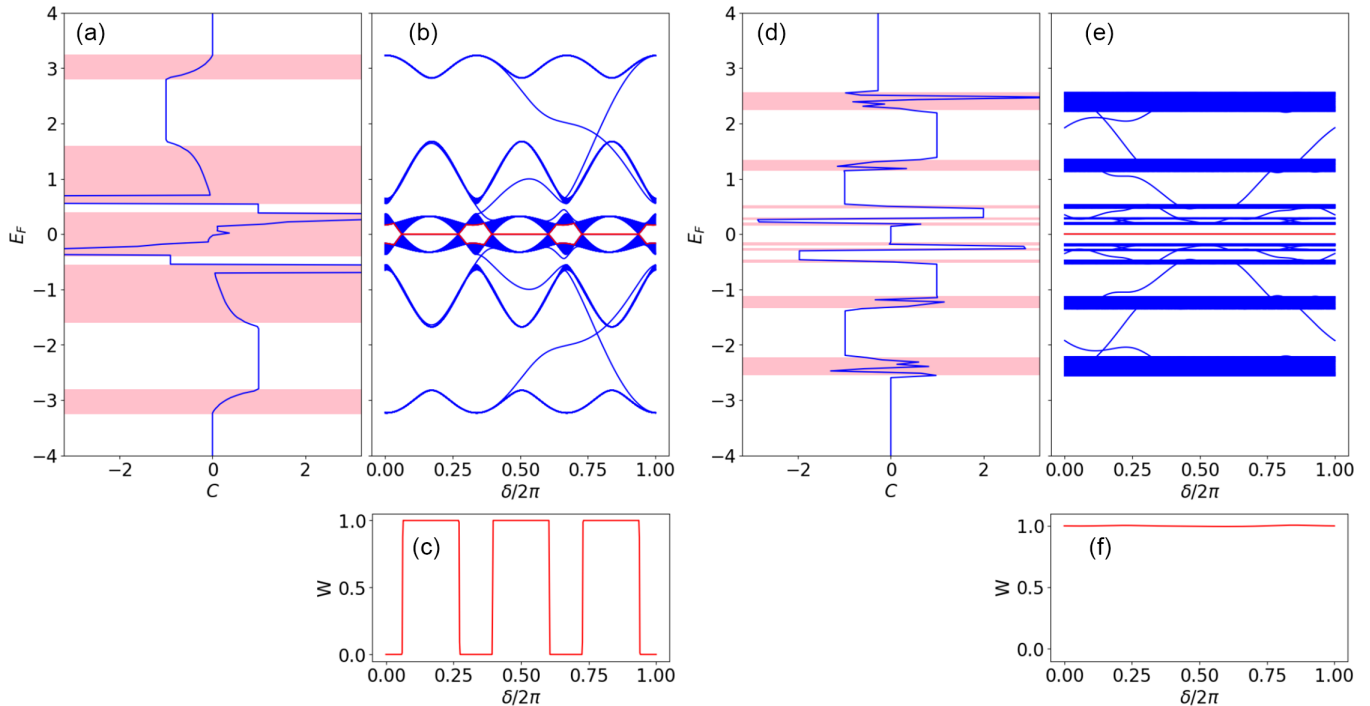


FIG. 7. Gap Chern numbers, energy spectrum, and winding number for a cAA model with a commensurate modulation [ $(b = 1/3)$  (a), (b) and (c) respectively], and with an incommensurate modulation [ $(b = 1/\tau)$  (d), (e) and (f) respectively]. Distinct topological phases are visible, with invariants  $(C, W) = (0, \pm 1)$ ,  $(1, \pm 1)$  in panels (a)–(c) as well as  $(C, W) = (1, \pm 1)$ ,  $(1, \pm 2)$ ,  $(1, \pm 3)$  in panels (d)–(f). The gap Chern numbers fluctuate within the regions marked in pink, where bulk bands are present, and converge to finite values within the bulk energy gaps.

enough  $q$ . This value then saturates for  $p/q$  approaching irrational values when the size of the unit cell induced by the modulation becomes comparable with the physical system size.

We have found that such a model can provide a platform for studying two different kinds of integer quantum Hall effect, namely when Dirac cones are present (a HIQHE similar to the case of graphene) or absent (the standard IQHE similar

to the square lattice). We find that it is possible to transition between the two by merging and splitting Dirac cones when the system's parameters are varied. Both types of IQHE are characterized by a Chern number, and when projected down to physical space from the superspace model, can lead to the localization of states at the edges, in correspondence with Landau levels in the superspace model.

The coexistence of zero-energy edge modes protected by the chiral symmetry and Landau-level edge states points to the exotic nature of the cAA, and the explicit computation of topological invariants all but confirms the coexistence, as we find that both invariants  $C$  and  $W$  are necessary to characterize the potential existence of edge states for a given physical realization of  $\delta$  and Fermi energy  $E_F$ . Furthermore, from the perspective of the 1D physical system, this coexistence means that it is possible, for small periodicities, to smoothly transform from 1D-type zero-energy edge modes located at both edges, to 2D-type Landau-level like finite-energy edge states, located at the same physical edge of the 1D chain.

Finally, much like other previously studied topological quasicrystals, an experimentally feasible implementation of the cAA could be studied using photonic crystals, where the hopping modulation could be achieved by controlling the spacing between distinct fiber optics [14,26]. In this setting, minimal changes to the way waveguides are spaced are necessary to realize the cAA model. Besides this one, many other alternatives exist, such as ultracold atom platforms, where generalized AA type models have been implemented in the past [46,47]; quantum simulators, using, for instance superconducting qubits [48], or other types of quantum

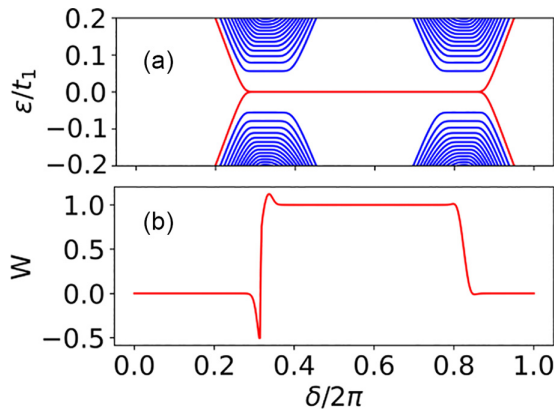


FIG. 8. (a) Emergence of Landau levels in the cAA model in a topological semimetal phase with two Dirac cones. We use the parameters  $t_1 = t_2 = \Delta_1 = 1$  and  $\Delta_2 = 0.5$  in a chain cAA chain with 600 atoms, and a periodicity or field  $b = 1/2001$ . (b) Winding number invariant, matching the presence of doubly degenerate edge modes, and changing with the presence of Dirac cones.

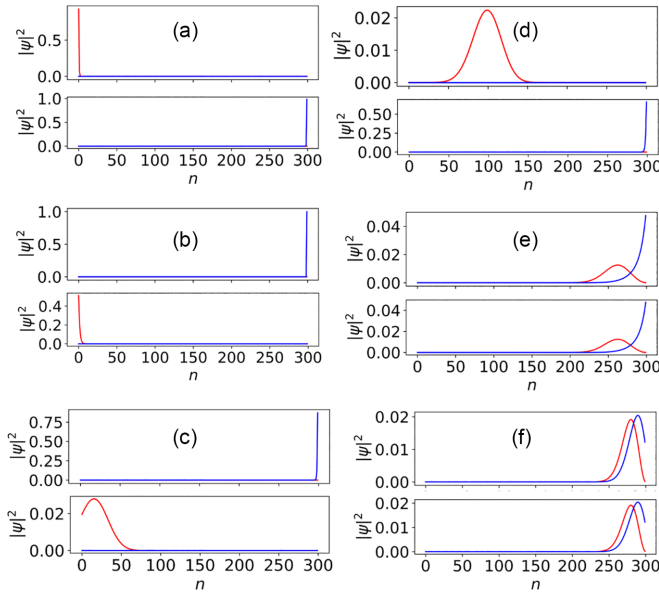


FIG. 9. Evolution of the doubly degenerate edge mode into a pair of nondegenerate Landau-level edge state as  $\delta$  is varied for parameters  $t_1 = t_2 = \Delta_1 = 1$  and  $\Delta_2 = 0.5$  in a chain cAA chain with 600 atoms, and a periodicity or field  $b = 1/2001$ . The phason is given by (a)  $\delta/2\pi = 0.59$ , (b)  $\delta/2\pi = 0.67$ , (c)  $\delta/2\pi = 0.75$ , (d)  $\delta = 0.80$ , (e)  $\delta = 0.88$ , (f)  $\delta = 0.92$ . The chiral symmetry of the 1D model initially ensures that the doubly degenerate edge modes at  $\varepsilon = 0$  in each of the two distinct sublattices (represented distinctly as blue and red curves) are located at both edges. By the time the degeneracy is lifted by shifting the phason  $\delta$ , the wave function is still supported in both sublattices but with distinct envelopes. One of the edge states is progressively brought towards the bulk and eventually both become localized at a single edge.

computational devices; and magnetic systems [29], with proposals existing for the realization of Aubry-André type systems taking advantage of twisted van der Waals heterostructures.

## ACKNOWLEDGMENTS

T.V.C.A. acknowledges support by the Portuguese Foundation for Science and Technology (FCT) in the framework of the Project No. CERN/FIS-COM/0004/2021 and the hospitality of LIP where this work was conducted. T.V.C.A. also acknowledges the computational resources provided by the Aalto Science-IT project. N.M.R.P. acknowledges support by the Portuguese Foundation for Science and Technology (FCT) in the framework of the Strategic Funding UIDB/04650/2020, COMPETE 2020, PORTUGAL 2020, FEDER, and through projects PTDC/FIS-MAC/2045/2021, EXPL/FIS-MAC/0953/2021, and from the European Commission through the project Graphene Driven Revolutions in ICT and Beyond (Ref. No. 881603, CORE 3). N.M.R.P. also acknowledges the Independent Research Fund Denmark (Grant No. 2032-00045B) and the Danish National Research Foundation (Project No. DNRF165).

## APPENDIX A: DETAILS OF THE SUPERSPACE MODEL IN THE VANISHING-FIELD LIMIT

In the main text we have presented the superspace model in the vanishing field limit without much discussion of its derivation. In this Appendix, we provide a quick and simple derivation, starting from the Hamiltonian, which realizes, for a fixed  $\delta$ , a physical implementation of the cAA model. It reads

$$H(\delta) = - \sum_n [t_1 + \Delta_1 \cos(2\pi bn - \delta)] a_n^\dagger b_n + [t_2 + \Delta_2 \cos(2\pi bn - \delta)] b_n^\dagger a_{n+1} + \text{H.c.} \quad (\text{A1})$$

The very simple trick, which allows us to generate the 2D superspace model is to expand the cosine modulations in terms of exponentials and allow, in the vanishing field limit  $b \rightarrow 0$ , the dependence on  $b$  to drop out from the Hamiltonian, yielding a  $b$ -independent Hamiltonian,

$$H(\delta) = - \sum_n \left[ t_1 + \frac{\Delta_1}{2} (e^{i\delta} + e^{-i\delta}) \right] a_n^\dagger b_n + \left[ t_2 + \frac{\Delta_2}{2} (e^{i\delta} + e^{-i\delta}) \right] b_n^\dagger a_{n+1} + \text{H.c.} \quad (\text{A2})$$

The fact that this form of the Hamiltonian is a good description of the model can be checked numerically, by setting, for instance  $b = 1/1001$ , which produces results for the 1D topology practically indistinct from the vanishing-field limit. The idea now is to imagine that  $\delta$  plays the role of a momentum variable, and promote the creation and annihilation operators into objects with two indices. The first is  $n$ , the lattice site along physical space, which for the sake of clarity we rename to  $i$  to better signify this change to a 2D model, and the second one is  $j$ , which is the position along the synthetic dimension, conjugate to the momentum  $\delta$ . So, our aim is to transform  $a_n^\dagger$  and  $b_n^\dagger$  as

$$a_n^\dagger \rightarrow \sum_j a_{i,j}^\dagger e^{-i\delta j}, \quad (\text{A3})$$

$$b_n^\dagger \rightarrow \sum_j b_{i,j}^\dagger e^{-i\delta j}, \quad (\text{A4})$$

and account for the already existing exponentials  $e^{\pm i\delta}$  as indicators of the existence of couplings in the synthetic direction. To see why this can be done, simply note that it is possible to write

$$\begin{aligned} a_i^\dagger b_i e^{-i\delta} &= \sum_{j,j'} b_{i,j'}^\dagger e^{-i\delta j'} a_{i,j} e^{i\delta j} e^{-i\delta} \\ &= \sum_{j,j'} b_{i,j'}^\dagger a_{i,j} e^{-i\delta(j'+1)} e^{i\delta j} \\ &= \sum_j b_{i,j}^\dagger a_{i,j+1}. \end{aligned} \quad (\text{A5})$$

Thus, the Hamiltonian of the system can be brought into 2D by splitting up the terms proportional to  $e^{\pm i\delta}$ , adding a summation in the synthetic dimension, an adjusting for the synthetic couplings generated as in Eq. (A5). This procedure results in Eq. (3) of the main text, which we repeat here for

convenience,

$$H_{2D} = - \sum_{i,j} t_1 a_{i,j}^\dagger b_{i,j} + \Delta'_1 a_{i,j}^\dagger b_{i,j+1} + \text{H.c.} \\ - \sum_{i,j} t_1 b_{i,j}^\dagger a_{i+1,j} + \Delta'_2 b_{i,j}^\dagger a_{i+1,j+1} + \text{H.c.} \quad (\text{A6})$$

This concludes our small derivation of the 2D superspace model in a “real space” representation. The generated hoppings are “diagonal” in the 2D lattice, as illustrated in Fig. 2 of the main text. Instead of choosing this representation, we can instead go into momentum space in both physical and synthetic dimensions. This amounts to performing the transformation

$$a_n^\dagger \rightarrow \sum_k a_k^\dagger e^{ikn}, \quad (\text{A7})$$

$$b_n^\dagger \rightarrow \sum_k b_k^\dagger e^{ikn}, \quad (\text{A8})$$

which leads to, summing over all possible values of  $\delta$  in order to take into account the synthetic dimension

$$H_{2D} = \sum_{k,\delta} [t_1 + \Delta_1 \cos \delta] a_k^\dagger b_k \\ + [t_2 + \Delta_2 \cos \delta] b_k^\dagger a_k e^{ik} + \text{H.c.} \quad (\text{A9})$$

A more convenient form is the Hamiltonian matrix, which was described in the main text

$$H_{2D}(\mathbf{k}) = - [t_1 + \Delta'_1 \cos \delta + (t_2 + \Delta'_2 \cos \delta) \cos k] \sigma_x \\ - [(t_2 + \Delta'_2 \cos \delta) \sin k] \sigma_y. \quad (\text{A10})$$

It is also worth remarking that the role played by the additional exponentials  $e^{\pm i2\pi bn}$  is to introduce additional phases along these hoppings, which explicitly break translational symmetry. Despite this, the position dependence on  $n$  is precisely what makes the system exactly mappable to an IQHE model in the Landau gauge. As we show in the main text, this limit can be analyzed numerically with topological markers.

## APPENDIX B: DIMENSIONAL REDUCTION AND AN ANALOGY WITH GRAPHENE

Underlying the cAA model and the richness of topological quasicrystals in general is the idea of synthetic dimensions. The procedure of mapping the cAA model into a superspace model involves taking a model parameter, in our case the modulation shift, and interpreting it as a momentum variable, thus generating a higher dimensional model with an additional synthetic dimension. The inverse procedure can be performed, and the role of this Appendix is to illustrate it via the example of graphene. We start with a physical 2D model and perform a process of dimensional reduction, by reinterpreting a momentum variable as an adjustable parameter.

Let us consider a zig-zag edge graphene ribbon. Like the cAA model, a zig-zag graphene ribbon has two sublattices  $A$  and  $B$  and, for a ribbon with  $N$  unit cells in the finite direction,

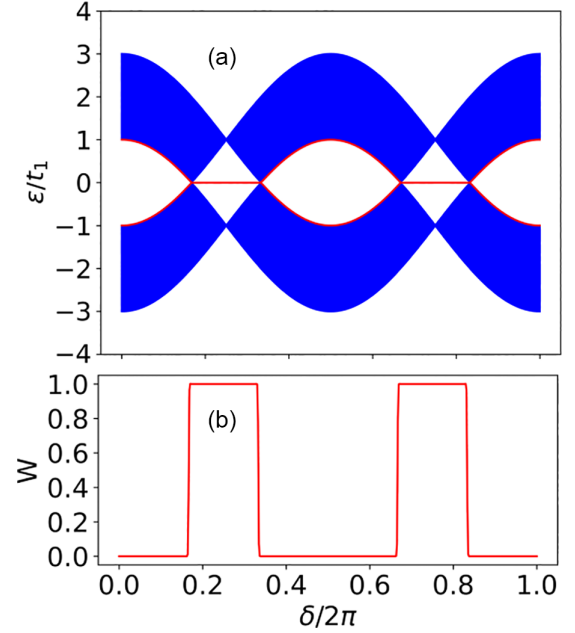


FIG. 10. (a) Energy spectrum for a graphene zig-zag ribbon, simulated using the cAA model. (b) Winding number of the SSH model resulting from dimensional reduction of the zig-zag graphene ribbon. We have  $W(\delta) = 1$  when doubly degenerate edge states are present, and  $W(\delta) = 0$  when the states wander into the bulk.

the Hamiltonian is of the form

$$H_g = -t \sum_{i=1}^{\infty} \sum_{j=1}^N a_{i,j}^\dagger b_{i,j} + b_{i,j}^\dagger a_{i,j+1} + b_{i,j}^\dagger a_{i+1,j} + \text{H.c.} \quad (\text{B1})$$

It is then possible to Fourier transform this Hamiltonian along the infinite direction, introducing the momentum variable  $k$ , resulting in

$$H_g = -t \sum_k \sum_{j=1}^N 2 \cos \left( \frac{\sqrt{3}}{2} k \right) a_{k,j}^\dagger b_{k,j} + b_{k,j}^\dagger a_{k,j+1} + \text{H.c.} \quad (\text{B2})$$

If we ignore the summation in  $k$ , the Hamiltonian is simply that of a finite SSH chain with hoppings modulated by the momentum  $k$ . Thus, from the 2D graphene lattice we have constructed a modulated 1D SSH model via a process of dimensional reduction. A winding number can be associated to this SSH model, and it indicates the presence of the characteristic degenerate edge modes at zero energy. This is a topological interpretation of this phenomena, which is often overlooked. In Fig. 10, we present the result of using the winding number topological marker presented in the main text to compute the topological invariant of the SSH model resulting from the dimensional reduction procedure when applied to a graphene zig-zag ribbon.

Finally, note that graphene can actually be mapped to a particular parameter set of the cAA model. By picking physical hoppings  $t_1 = \Delta_2 = 0$ ,  $t_2 = t$ , and  $\Delta_1 = 2t$ , as well as a value of  $b = 0$  and identifying  $\sqrt{3}k/2$  with the shift  $\delta$ , we can simulate graphene in the cAA model. Since graphene appears in the limit of  $b = 0$ , the parameter  $\delta$  does not exactly play the role of a shift of the potential, but rather, by itself, it globally

reduces or increases the strength of the intracell hopping. The connection between these models therefore definitely exists; however, the fact that no actual Aubry-André periodic modulation is present removes many of the puzzling features of the cAA model. Nonetheless, this correspondence establishes

that the concept of synthetic dimensions can be utilized, in principle, to simulate a graphene lattice in a 1D model, by accessing slices of its spectrum, and tuning the tight-binding hopping strengths in order to move around the momentum direction.

- 
- [1] D. Shechtman, I. Blech, D. Gratias, and J. W. Cahn, Metallic phase with long-range orientational order and no translational symmetry, *Phys. Rev. Lett.* **53**, 1951 (1984).
- [2] E. Maciá, The role of aperiodic order in science and technology, *Rep. Prog. Phys.* **69**, 397 (2006).
- [3] P. J. Steinhardt and S. Ostlund, *The Physics of Quasicrystals* (World Scientific, Singapore, 1987).
- [4] M. Senechal, *Quasicrystals and Geometry* (Cambridge University Press, Cambridge, 1995).
- [5] M. Duneau and A. Katz, Quasiperiodic patterns, *Phys. Rev. Lett.* **54**, 2688 (1985).
- [6] V. Elser and C. L. Henley, Crystal and quasicrystal structures in Al-Mn-Si alloys, *Phys. Rev. Lett.* **55**, 2883 (1985).
- [7] A. Jagannathan, The fibonacci quasicrystal: Case study of hidden dimensions and multifractality, *Rev. Mod. Phys.* **93**, 045001 (2021).
- [8] N. G. de Bruijn, Algebraic theory of Penrose's non-periodic tilings of the plane. II, *Indagationes Mathematicae (Proceedings)* **84**, 53 (1981).
- [9] P. Moon, M. Koshino, and Y.-W. Son, Quasicrystalline electronic states in 30° rotated twisted bilayer graphene, *Phys. Rev. B* **99**, 165430 (2019).
- [10] B. Amorim, F. Riche, E. Castro, P. Ribeiro, and M. Gonçalves, Incommensurability enabled quasi-fractal order in 1D narrow-band moiré systems, [arXiv:2305.03800](https://arxiv.org/abs/2305.03800).
- [11] J. A. Crosse and Pilkyung Moon, Quasicrystalline electronic states in twisted bilayers and the effects of interlayer and sublattice symmetries, *Phys. Rev. B* **103**, 045408 (2021).
- [12] Ang-Kun Wu, Fractal spectrum of the Aubry-Andre model, [arXiv:2109.07062v2](https://arxiv.org/abs/2109.07062v2).
- [13] G. A. Domínguez-Castro and R. Paredes, The aubry-andré model as the hobbyhorse for understanding localization phenomenon, *Eur. J. Phys.* **40**, 045403 (2019).
- [14] Y. E. Kraus, Y. Lahini, Z. Ringel, M. Verbin, and O. Zilberberg, Topological states and adiabatic pumping in quasicrystals, *Phys. Rev. Lett.* **109**, 106402 (2012).
- [15] Y. E. Kraus, Z. Ringel, and O. Zilberberg, Four-dimensional quantum Hall effect in a two-dimensional quasicrystal, *Phys. Rev. Lett.* **111**, 226401 (2013).
- [16] M. Lohse, C. Schweizer, H. M. Price, O. Zilberberg, and I. Bloch, Exploring 4D quantum Hall physics with a 2D topological charge pump, *Nature (London)* **553**, 55 (2018).
- [17] E. Prodan, Virtual topological insulators with real quantized physics, *Phys. Rev. B* **91**, 245104 (2015).
- [18] D. R. Hofstadter, Energy levels and wave functions of bloch electrons in rational and irrational magnetic fields, *Phys. Rev. B* **14**, 2239 (1976).
- [19] K. v. Klitzing, G. Dorda, and M. Pepper, New method for high-accuracy determination of the fine-structure constant based on quantized Hall resistance, *Phys. Rev. Lett.* **45**, 494 (1980).
- [20] Y. Hatsugai, Chern number and edge states in the integer quantum Hall effect, *Phys. Rev. Lett.* **71**, 3697 (1993).
- [21] D. J. Thouless, M. Kohmoto, M. P. Nightingale, and M. den Nijs, Quantized Hall conductance in a two-dimensional periodic potential, *Phys. Rev. Lett.* **49**, 405 (1982).
- [22] D. V. Else, S.-J. Huang, A. Prem, and A. Gromov, Quantum many-body topology of quasicrystals, *Phys. Rev. X* **11**, 041051 (2021).
- [23] J. Zurita, C. Creffield, and G. Platero, Tunable zero modes and quantum interferences in flat-band topological insulators, *Quantum* **5**, 591 (2021).
- [24] S. Ganeshan and S. Das Sarma, Constructing a Weyl semimetal by stacking one-dimensional topological phases, *Phys. Rev. B* **91**, 125438 (2015).
- [25] P. Rosenberg and E. Manousakis, Topological superconductivity in a two-dimensional Weyl SSH model, *Phys. Rev. B* **106**, 054511 (2022).
- [26] S. Longhi, Topological Anderson phase in quasi-periodic waveguide lattices, *Opt. Lett.* **45**, 4036 (2020).
- [27] P. Molignini, A. G. Celades, R. Chitra, and W. Chen, Crossdimensional universality classes in static and periodically driven Kitaev models, *Phys. Rev. B* **103**, 184507 (2021).
- [28] W.-P. Su, J. R. Schrieffer, and A. J. Heeger, Solitons in polyacetylene, *Phys. Rev. Lett.* **42**, 1698 (1979).
- [29] J. L. Lado and O. Zilberberg, Topological spin excitations in Harper-Heisenberg spin chains, *Phys. Rev. Res.* **1**, 033009 (2019).
- [30] Y. E. Kraus and O. Zilberberg, Topological equivalence between the fibonacci quasicrystal and the Harper model, *Phys. Rev. Lett.* **109**, 116404 (2012).
- [31] A. H. Castro Neto, F. Guinea, N. M. R. Peres, K. S. Novoselov, and A. K. Geim, The electronic properties of graphene, *Rev. Mod. Phys.* **81**, 109 (2009).
- [32] A. Kitaev, Anyons in an exactly solved model and beyond, *Ann. Phys.* **321**, 2 (2006).
- [33] R. Bianco and R. Resta, Mapping topological order in coordinate space, *Phys. Rev. B* **84**, 241106 (2011).
- [34] G. von Gersdorff, S. Panahyan, and W. Chen, Unification of topological invariants in Dirac models, *Phys. Rev. B* **103**, 245146 (2021).
- [35] W. Chen, Universal topological marker, *Phys. Rev. B* **107**, 045111 (2023).
- [36] J. Sykes and R. Barnett, 1D quasicrystals and topological markers, *Mater. Quantum. Technol.* **2**, 025005 (2022).
- [37] A. Altland and M. R. Zirnbauer, Nonstandard symmetry classes in mesoscopic normal-superconducting hybrid structures, *Phys. Rev. B* **55**, 1142 (1997).
- [38] S. Ryu, A. P. Schnyder, A. Furusaki, and A. W. W. Ludwig, Topological insulators and superconductors: Tenfold way and dimensional hierarchy, *New J. Phys.* **12**, 065010 (2010).

- [39] J. N. B. Rodrigues and P. A. D. Gonçalves and N. F. G. Rodrigues and R. M. Ribeiro and J. M. B. Lopes dos Santos and N. M. R. Peres, Zigzag graphene nanoribbon edge reconstruction with Stone-Wales defects, *Phys. Rev. B* **84**, 155435 (2011).
- [40] H. B. Nielsen and M. Ninomiya, Absence of neutrinos on a lattice, *Nucl. Phys. B* **185**, 20 (1981).
- [41] H. B. Nielsen and M. Ninomiya, Absence of neutrinos on a lattice, *Nucl. Phys. B* **193**, 173 (1981).
- [42] Y. S. Krivosenko, I. V. Iorsh, and I. A. Shelykh, Bosonic Hofstadter butterflies in synthetic antiferromagnetic patterns, *J. Phys.: Condens. Matter* **33**, 135802 (2021).
- [43] D. J. Thouless, Quantization of particle transport, *Phys. Rev. B* **27**, 6083 (1983).
- [44] D. Vanderbilt, *Berry Phases in Electronic Structure Theory* (Cambridge University Press, Cambridge, 2018).
- [45] N. A. Spaldin, A beginner's guide to the modern theory of polarization, *J. Solid State Chem.* **195**, 2 (2012).
- [46] K. K. Das and J. Christ, Realizing the harper model with ultracold atoms in a ring lattice, *Phys. Rev. A* **99**, 013604 (2019).
- [47] Y. Li, J.-H. Zhang, F. Mei, J. Ma, L. Xiao, and S. Jia, Generalized Aubry-André-Harper models in optical superlattices, *Chin. Phys. Lett.* **39**, 063701 (2022).
- [48] H. Li, Y.-Y. Wang, Y.-H. Shi, K. Huang, X. Song, G.-H. Liang, Z.-Y. Mei, B. Zhou, H. Zhang, J.-C. Zhang *et al.*, Observation of critical phase transition in a generalized Aubry-André-Harper model with superconducting circuits, *npj Quantum Inf.* **9**, 40 (2023).